Available online at www.sciencedirect.com
ScienceDirect
International Journal of Multiphase Flow 33 (2007) 545–556
International Journal of Multiphase Flow
www.elsevier.com/locate/ijmulflow

A parametric study of droplet deformation through a microfluidic contraction: Shear thinning liquids

D.J.E. Harvie [a,*], M.R. Davidson [a], J.J. Cooper-White [b], M. Rudman [c]

[a] Department of Chemical and Biomolecular Engineering, University of Melbourne, Victoria 3010, Australia
[b] Division of Chemical Engineering, University of Queensland, Queensland 4072, Australia
[c] CSIRO Manufacturing and Infrastructure Technology, P.O. Box 56, Highett, Victoria 3190, Australia

Received 10 July 2006; received in revised form 16 November 2006

Abstract

Numerical simulations of a droplet passing through an axisymmetric microfluidic contraction are presented, focusing on systems where one of the two liquids present is shear thinning. The simulations are performed using a transient Volume of Fluid (VOF) algorithm. When the droplet is shear thinning and the surrounding phase Newtonian, droplets deform in a similar way to Newtonian droplets that have a viscosity equal to the average viscosity of the shear thinning fluid while it is within the contraction. When the surrounding phase is shear thinning and the droplet Newtonian, droplets deform in a similar way to droplets contained within a Newtonian liquid that has a viscosity that is lower than that of the droplet. In both cases the behaviour of the shear thinning fluid can be broadly described in terms of a 'characteristic' Newtonian viscosity: However, determining the exact value of this viscosity without performing a full shear thinning simulation is not possible.

Keywords: Volume of Fluid; Shear thinning; Contraction; Microfluidics; Non-Newtonian; Droplet; Carreau

1. Introduction

Microfluidic technology has the potential to revolutionise chemical and biological analysis and processing in the same way that integrated circuit technology revolutionised data analysis and processing three decades ago (Squires and Quake, 2005). As microfluidic processes operate on small length scales they generally consume smaller amounts of sample, require less time, and are easier to automate and control than more conventionally sized processes. How droplets behave within such microfluidic devices has application in the biotechnology, food, cosmetic and pharmaceutical industries. For example: reagents in chemical and biological assays that are constrained within droplets can be mixed by shear as the droplets move through a network (Song and Ismagilov, 2003); extrusion of liquid filaments through concentric contractions can be used to

* Corresponding author. Tel.: +61 03 83446618; fax: +61 03 83444153.
E-mail address: daltonh@unimelb.edu.au (D.J.E. Harvie).

0301-9322/$ - see front matter © 2007 Elsevier Ltd. All rights reserved.
doi:10.1016/j.ijmultiphaseflow.2006.12.002

produce micron-sized fibres (Jeong et al., 2004); breakup of a liquid stream in a contraction (flow focusing) can be used as an emulsification technique (Anna et al., 2002; Utada et al., 2005).

A microfluidic contraction is chosen as the representative geometry in this study as it is simple, contains strong but distinct regions of extensional and shear strain, and is able to deform a droplet's shape considerably. Previously, the authors presented numerical studies of droplet deformation for Newtonian fluids passing through a 4:1 axisymmetric contraction (Harvie et al., 2005, 2006). In this study we continue our examination of droplet behaviour within a microfluidic contraction, but focus on systems that contain a shear thinning fluid. Such fluids are abundant in industrial and biological fields. They include various polymer suspensions and melts (Bird et al., 1987; Barnes et al., 1989; Tanner, 2000), as well as suspensions of organic products such as blood (Gijsen et al., 1998). Understanding how biological fluids behave within microfluidic devices has particular application to biomedical 'Lab-on-a-chip' design.

Previous works concerned with the movement of droplets through contractions have usually considered only Newtonian fluids. Typical of these are the numerical studies of Tsai and Miksis (1997), Khayat et al. (1997, 2000) and Aboubacar et al. (2002), and the experimental studies of Anna et al. (2002) and Sugiura et al. (2002). A more complete review of the literature in this field is given in Harvie et al. (2006). The authors are not aware of any studies involving droplets passing through contractions where one of the fluids present is shear thinning. The single phase problem of a shear thinning fluid moving into a contraction has been considered both experimentally and numerically (see for example Kim-E et al., 1983). Droplet deformation in general extensional and shear flows has been extensively studied. Eggers (1997) and Stone (1994) give reviews of this topic.

The purpose of this study is to analyse the effect that the Reynolds number, surface tension strength and shear thinning fluid characteristics have on the deformation of a droplet as it passes through an axisymmetric contraction. We consider systems where either the disperse phase is shear thinning and the continuous phase is Newtonian, or where the continuous phase is shear thinning and the disperse phase Newtonian. We simulate parameter ranges that are relevant to liquid–liquid systems and characteristic of microfluidic applications, and perform the simulations using a transient Volume of Fluid (VOF) finite volume algorithm.

2. Mathematical model

Three non-dimensional equations are used to describe motion throughout the disperse (i.e., droplet) and continuous (i.e., surrounding) phases; a continuity equation, a volume-averaged incompressible Navier–Stokes momentum equation, and an advection equation which describes the evolution of the disperse phase volume fraction ϕ,

$$\nabla \cdot \boldsymbol{u} = 0 \tag{1}$$

$$\frac{\partial \rho \boldsymbol{u}}{\partial t} + \nabla \cdot \rho \boldsymbol{u}\boldsymbol{u} = -\nabla p + \frac{1}{We}\kappa\delta(\boldsymbol{x} - \boldsymbol{x}_s)\boldsymbol{n} + \frac{1}{Re}\nabla \cdot \mu[\nabla \boldsymbol{u} + (\nabla \boldsymbol{u})^T] \tag{2}$$

$$\frac{\partial \phi}{\partial t} + \nabla \cdot \phi \boldsymbol{u} = 0 \tag{3}$$

These equations are fairly conventional, except possibly for the second term on the right of Eq. (2) which represents the surface tension induced stress jump which occurs across any disperse–continuous phase interface. In this term κ is the signed local curvature of the interface, $\delta(\boldsymbol{x} - \boldsymbol{x}_s)$ is the Dirac delta function, non-zero only on the interface (i.e., at $\boldsymbol{x}_s$), and $\boldsymbol{n}$ is a unit vector directed normal to the interface and into the disperse phase. Gravitational forces have been neglected as their effect in micro-sized flows is small. Velocity is scaled by the average inlet velocity v^*, length by the radius of the inlet pipe R^* and density by the continuous phase density ρ_c^*. Viscosity is scaled by the maximum viscosity of any Newtonian phase that is present, μ_{max}^*. If only one Newtonian phase is present, then μ_{max}^* equals the viscosity of that phase. If both phases are Newtonian then $\mu_{max}^* = \max(\mu_d^*, \mu_c^*)$. Note that an asterix in our notation implies a dimensioned quantity, and the subscripts 'd' and 'c' refer to the disperse and continuous phases, respectively.

Both μ and ρ used in Eq. (2) represent local, volume-averaged quantities. As the focus of this study is on liquid–liquid systems, the density is set to be equal in both phases so that $\rho = \rho^*/\rho_c^* = 1$ everywhere. Local

values of μ depend on the local volume fraction, ϕ, via $\mu = \phi\mu_d + (1-\phi)\mu_c$, where μ_d and μ_c are the local, non-dimensional phase viscosities: In Newtonian phases these viscosities are constant, but in shear thinning phases they depend on the local shear rate.

For shear thinning fluids we use the Carreau model to describe the viscosity of that phase (Bird et al., 1987). The Carreau model relates the local non-dimensional phase viscosity μ_{st} (=μ_d or μ_c) to a non-dimensional 'infinite shear rate' viscosity μ_∞ via

$$\frac{\mu_{st}-\mu_\infty}{1-\mu_\infty} = [1+(\lambda\dot{\gamma})^2]^{(n-1)/2} \tag{4}$$

where λ is a time constant, n is a 'power-law exponent' and the total shear rate is given by $\dot{\gamma} = \sqrt{\nabla\boldsymbol{u} : [\nabla\boldsymbol{u} + (\nabla\boldsymbol{u})^T]}$. Eq. (4) has been non-dimensionalised so that $\mu_{st} = 1$ when the shear rate is zero. This means that the 'zero shear rate' viscosity of any shear thinning fluid used in this study is set equal to the viscosity of the companion Newtonian fluid. Thus, local shear thinning viscosities are constrained to be less than or equal to the viscosity of the companion Newtonian fluid.

The Reynolds (Re) and Weber (We) numbers appearing in Eq. (2), along with the related capillary (Ca) number, are defined as

$$Re = \frac{\rho_c^* v^* R^*}{\mu_{max}^*}, \quad We = \frac{\rho_c^* v^{*2} R^*}{\sigma^*}, \quad \text{and} \quad Ca = \frac{We}{Re} = \frac{v^*\mu_{max}^*}{\sigma^*}$$

The results are presented in terms of Re and a 'surface tension number'

$$S = \frac{1}{We+Ca} = \frac{\sigma^*}{v^*\mu_{max}^* + \rho_c^* v^{*2} R^*}$$

which is an appropriate measure of surface tension strength for both large and small values of Re (Harvie et al., 2006).

3. Problem description and simulation method

The deformation of a droplet passing through a 4:1 axisymmetric contraction was considered (Fig. 1). The inlet velocity profile was taken to be that of fully developed Poiseuille flow based on the continuous phase zero shear rate viscosity; droplet deformation behaviour was found to be quite insensitive to the choice of this profile however. The pressure gradient normal to the outlet was chosen to ensure overall mass conservation. No-slip boundary conditions were applied at the channel walls, which were also assumed to be non-wetting with respect to the droplet phase. The simulations were performed using an adapted form of the VOF finite volume algorithm of Rudman (1998). This code was also used in the companion studies of Harvie et al. (2005, 2006). The extension to shear thinning (generalised Newtonian) fluids was implemented by Davidson and Cooper-White (2006) in relation to pendant drops.

For all of the simulations presented a mesh of dimensions 64×768 was used. This mesh resolution was found to give a good compromise between simulation accuracy and computational time. A mesh sensitivity analysis similar to that presented in Harvie et al. (2006) showed that at this mesh density, the overall form

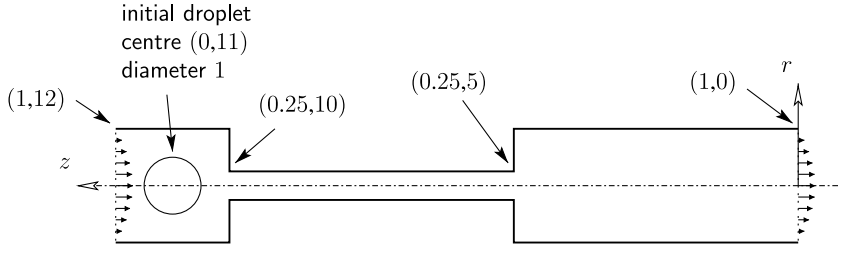

Fig. 1. The geometry used in the computational problem. All lengths are normalised by the inlet radius R^* and cylindrical coordinates (r,z) are used.

of droplet deformation predicted by the simulations is mesh independent. Smaller scale features present in the more topologically complex simulations, such as individual interface instabilities or individual pieces of small scale debris produced as the droplet exits the contraction, are not predicted quantitatively at this mesh resolution, but their presence and general characteristics are. Thus, qualitative conclusions can be drawn about the small scale behaviour of droplets from the results, and quantitative conclusions about the overall droplet behaviour.

4. Results: shear thinning disperse phase

Fig. 2a shows images of a shear thinning droplet that is contained within a Newtonian continuous phase and passing through the contraction. For this simulation $Re = 4.12 \times 10^{-2}$ and $S = 3.97 \times 10^{-1}$, thus, viscous forces generally dominate inertial forces and surface tension forces are of a comparable magnitude to the other forces acting in the system. For the shear thinning disperse phase, the Carreau parameters used were $\mu_{d,\infty} = 0$, $\lambda = 1$ and $n = 0.6$. As shown in Fig. 3, the viscosity of this fluid is approximately one when the total shear rate is below one, but decreases quite rapidly as the shear rate increases above this level. The images show that the form of the droplet changes from a sphere to an elongated filament as it enters the contraction, and returns to a semi-spherical shape with a 'stub' rear after leaving the contraction. The tail of the droplet adopts a distinctive 'forked' shape as it passes through the contraction.

Comparing the results of Fig. 2a against Newtonian droplet results presented previously shows that the behaviour of this droplet is similar to that of a low viscosity Newtonian droplet passing through the same

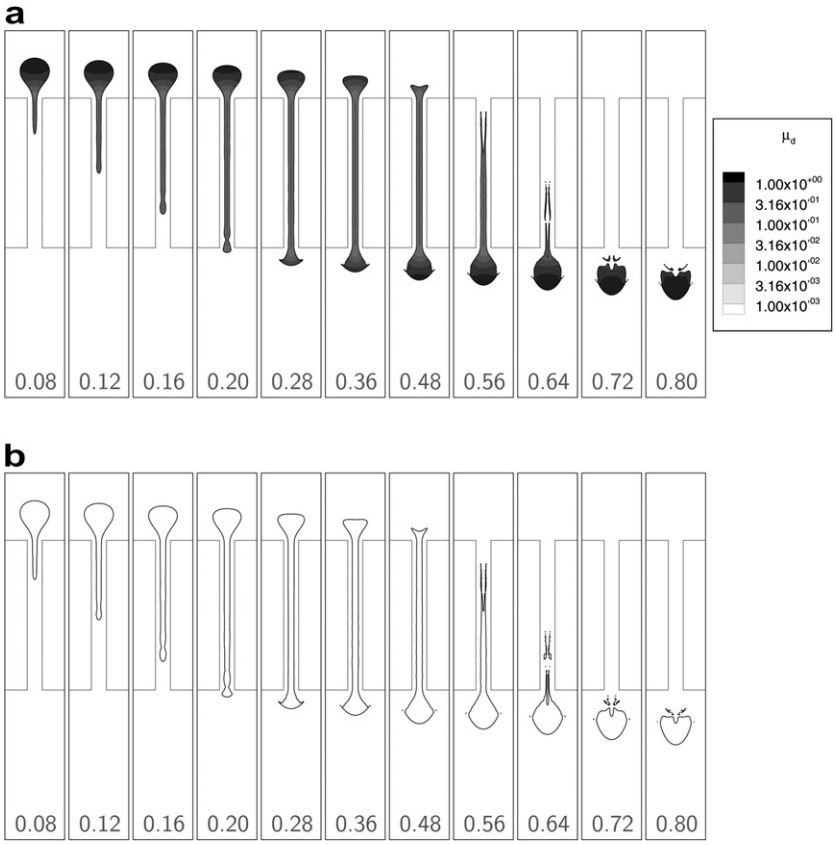

Fig. 2. Images from simulations conducted with $Re = 4.12 \times 10^{-2}$ and $S = 3.97 \times 10^{-1}$. In each image fluid flows from top to bottom and simulation times are indicated at the bottom of each frame. In both cases the continuous phase is Newtonian. In the shear thinning case the shading represents the local viscosity. (a) Shear thinning disperse phase with $\mu_{d,\infty} = 0$, $\lambda = 1$ and $n = 0.2$ and (b) Newtonian continuous phase with $\mu_d = 0.1$.

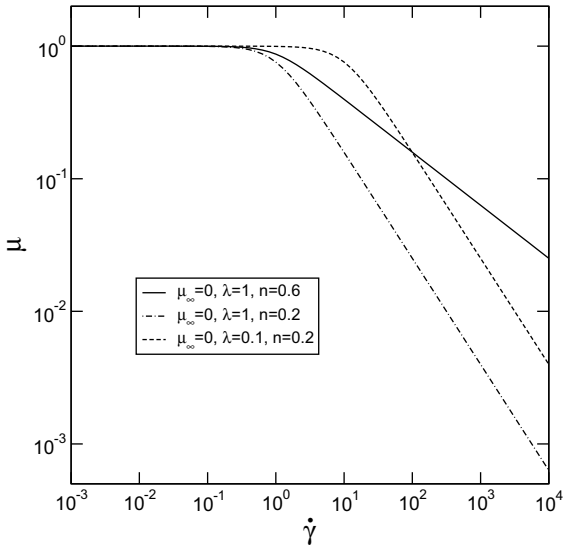

Fig. 3. Shear thinning viscosity (μ_{st}) as a function of total shear rate ($\dot{\gamma}$) for a variety of Carreau model parameters.

contraction (Harvie et al., 2006). This suggests that using a Newtonian droplet to approximate the behaviour of a shear thinning droplet may be feasible provided that an appropriate viscosity is chosen for the Newtonian drop. Examining Fig. 2b, we see that when the shear thinning droplet is within the contraction, the viscosity of the disperse phase is reasonably uniform at $\mu_d = \mu_d^*/\mu_c^* \approx 0.1$. Fig. 2b shows results from a simulation that is identical to that of Fig. 2a, but where a Newtonian droplet of this viscosity ($\mu_d = 0.1$) has been used.

Comparing the two simulations shows that the behaviour of the droplets is very similar, especially when they are entering, are within, or are exiting the contraction. So for the example of Fig. 2b, the behaviour of the shear thinning droplet is substantially described by a single Newtonian 'characteristic' viscosity, taken to be the average shear thinning viscosity of the droplet while it is within the contraction.

While the behaviour of this shear thinning droplet is reasonably well described by a single characteristic viscosity, unfortunately it is not possible to predict the magnitude of this viscosity without performing a shear thinning simulation. We can calculate a range in which this characteristic viscosity should lie however using results from a Newtonian simulation.

To demonstrate, consider Fig. 4, which shows the steady-state total shear rate experienced around the entrance to the contraction when only a Newtonian fluid of viscosity $\mu = 1$ is present. For this figure the Reynolds number is the same as that used in Fig. 2a. If we equate the average shear rate that the Newtonian fluid experiences within the contraction ($\dot{\gamma} \approx 1 \times 10^2$) to the shear rate that a shear thinning droplet would experience while within the contraction, we get an upper estimate for the characteristic viscosity of $\mu_d \approx 0.16$. This is an upper limit to the characteristic viscosity as the shear rate that a real shear thinning fluid would experience while within the contraction would be higher than given by Fig. 4, because the viscosity of a shear thinning fluid at finite shear rates is less than that of our Newtonian fluid.

If instead we equate the magnitude of stress that the Newtonian fluid experiences while within the contraction ($\tau \approx 1 \times 10^2$) to the stress that a shear thinning fluid would experience while within the contraction ($\tau \approx \dot{\gamma}\mu$ in an order of magnitude sense), we get a lower estimate for the characteristic viscosity of $\mu_d \approx 0.046$. In calculating this value we have used Eq. (4) to relate the viscosity and shear rate of the shear thinning fluid. This viscosity is a lower limit to the characteristic viscosity as the stress that would exist in an actual shear thinning fluid would be lower than indicated by Fig. 4, as the viscosity of a shear thinning fluid is less than that of our Newtonian fluid.

So, although it is not possible to calculate the characteristic viscosity without performing a shear thinning simulation, it is possible to estimate a range in which it will lie using results from a Newtonian fluid simulation. Clearly for the example shown in Fig. 2a the chosen characteristic viscosity of $\mu_d = 0.1$ lies within the calculated range of $0.046 < \mu_d < 0.16$.

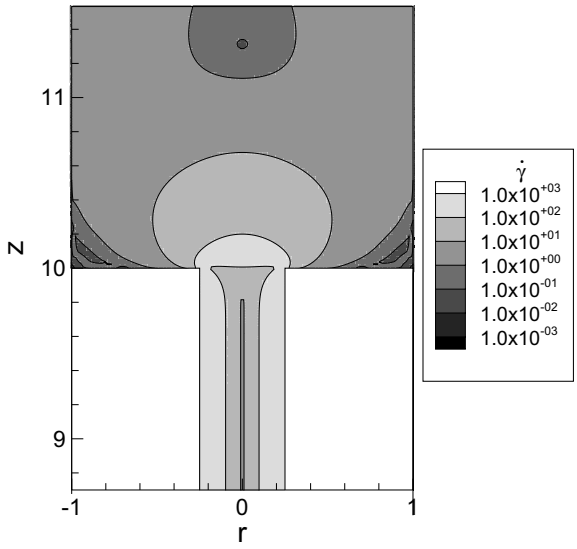

Fig. 4. Total shear rate ($\dot{\gamma}$) at the entrance to the contraction in the absence of the droplet. Here $Re = 4.12 \times 10^{-2}$.

Fig. 5a shows images from a simulation conducted with the same values of Re and S as used in Fig. 2a, but with the altered Carreau parameters of $\mu_{d,\infty} = 0$, $\lambda = 1$ and $n = 0.2$. The 'power-law exponent' has been decreased from $n = 0.6$ to 0.2 here so that the droplet fluid thins more rapidly with shear rate than previously (see Fig. 3). These Carreau parameters could represent the viscosity of a semi-dilute suspension of polystyrene spheres (Bird et al., 1987).

In terms of the contraction problem, the decrease in n means that the disperse phase viscosity decreases more as the droplet enters the contraction than previously, and as a result, the characteristic viscosity for this example is lower: The average viscosity of the droplet while it is within the contraction is around $\mu_d = 0.001$. Unsurprisingly then, the behaviour of this droplet as it enters, is within, and exits the contraction is similar to that of a Newtonian droplet with a viscosity of $\mu_d = 0.001$, as shown in Fig. 5b. Note that using the methods outlined previously, the range in which the characteristic viscosity should lie based on the Newtonian results of Fig. 4 is $1 \times 10^{-7} < \mu_d < 0.025$. This range includes the characteristic viscosity calculated using the full shear thinning simulation.

One interesting feature of shear thinning fluids that is evident in Fig. 5a is that the viscosity of a shear thinning fluid generally decreases more than one might expect based on Newtonian strain rate calculations. Between $t \approx 0.2$ and $t \approx 0.48$ in Fig. 5a for example, although the strain rates calculated within the Newtonian continuous phase in the outlet region are quite low, strain rates calculated within the disperse phase in this region are high, resulting in a low disperse phase viscosity. This is why the droplet of Fig. 5a behaves so similarly to the Newtonian droplet of Fig. 5b within the outlet region despite the surrounding strain rates being low. Indeed, differences in behaviour between the two droplets only become apparent after the leading tips have moved a considerable distance from the contraction, and the viscosity of the shear thinning droplet increases in response to very low levels of applied stress from the continuous phase.

Strong interface instability growth is evident in the simulations of Fig. 5a and b. The instabilities that develop on these droplets while they are within the contraction are driven by shear stresses that act across the interface of the droplet, but grow from perturbations applied to the droplet's diameter by flow oscillations that exist at the entrance to the contraction. The nature of these instabilities is discussed in detail in Harvie et al. (2006) where they were observed on low viscosity Newtonian droplets passing through the same contraction.

The simulation shown in Fig. 5c uses the same Re and S as used previously, but now the Carreau parameters of $\mu_{d,\infty} = 0$, $\lambda = 0.1$ and $n = 0.2$ for the disperse phase. Thus, this fluid has a smaller time constant λ than in previous cases, and referring to Fig. 3, begins shear thinning at a higher total shear rate than the other

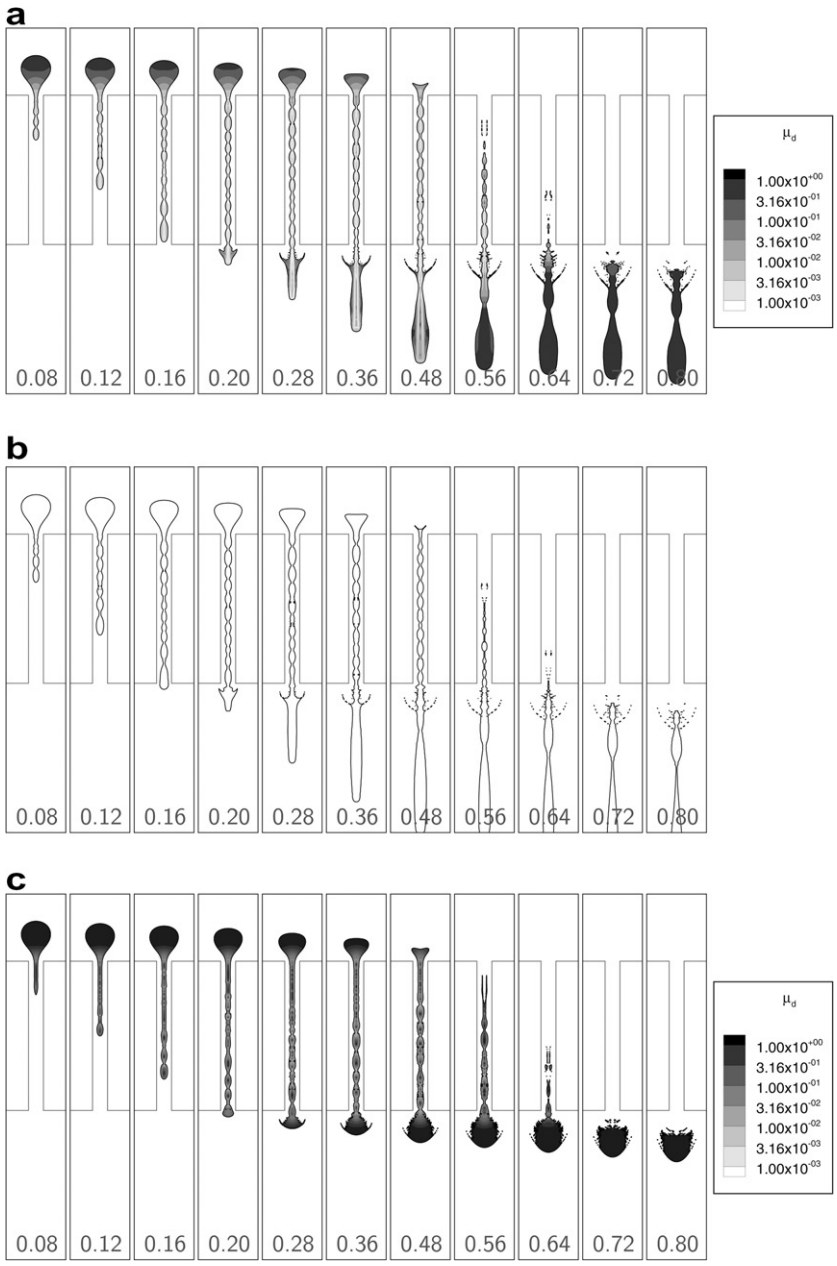

Fig. 5. Images from simulations conducted with $Re = 4.12 \times 10^{-2}$ and $S = 3.97 \times 10^{-1}$. In each image fluid flows from top to bottom and simulation times are indicated at the bottom of each frame. In all cases the continuous phase is Newtonian. In the shear thinning cases the shading represents the local viscosity. (a) Shear thinning continuous phase with $\mu_{d,\infty} = 0$, $\lambda = 1$ and $n = 0.2$, (b) Newtonian disperse phase with $\mu_d = 0.001$ and (c) shear thinning disperse phase with $\mu_{d,\infty} = 0$, $\lambda = 1$ and $n = 0.2$.

fluids; however, at high total shear rates it shear thins at the same rate as the fluid used in Fig. 5a. As a result, the droplet in Fig. 5c is generally more viscous while within the contraction than the droplet in Fig. 5a, but generally less viscous while within the contraction than the droplet in Fig. 2a. As one might expect then, the behaviour of this droplet shares similarities with both of the previous shear thinning droplets: Within the contraction some medium wavelength instability growth is evident, as in the case of Fig. 5a, but due to the higher local viscosities present the disturbances take more time to grow and are less pronounced over the length of the filament; Beyond the contraction, the droplet forms the 'stubby' rear spherical shape as previously seen in

the case of Fig. 2a, but now the instabilities that were present on the droplet when it was in the contraction expand radially as it exits the contraction to form a layer of small scale debris surrounding the droplet in the final timeframe. As the droplet proceeds towards the outlet much of this debris combines with the bulk of the droplet fluid again. However, as with the previous simulations, the finite resolution of the mesh means that these small scale events may not be accurately predicted (Harvie et al., 2006).

As well as the simulations already presented, a large number of other simulations were conducted using a variety of shear thinning Carreau parameters for the disperse phase, together with a variety of the *Re* and *S* numbers as employed in the previous studies (Harvie et al., 2005, 2006). Consistent with the above these droplets generally behaved as Newtonian droplets do at a (characteristic) viscosity equal to the average viscosity of the shear thinning fluid while within the contraction.

5. Results: shear thinning continuous phase

Fig. 6a shows a simulation conducted with the same *Re* and *S* as used in the simulations of Figs. 2 and 5, but now with a shear thinning continuous phase and Newtonian disperse phase. The Carreau parameters are the same as those used in Fig. 5a, that is, $\mu_{c,\infty} = 0$, $\lambda = 1.0$ and $n = 0.2$. The behaviour of this droplet is quite different to that observed in the shear thinning disperse phase simulations: The droplet deforms less prior to entering the contraction; appears to 'contact' the contraction 'lip' as it enters the contraction; and leaves a thin film of slowly moving droplet liquid along the solid wall long after the majority of the disperse phase liquid has passed through the contraction.

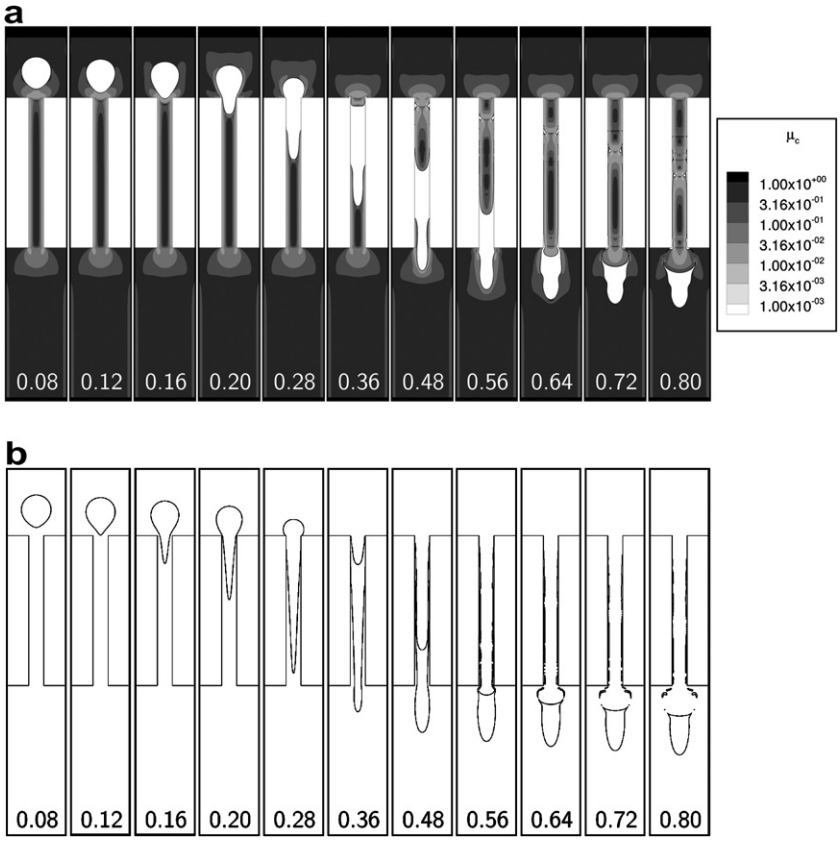

Fig. 6. Images from simulations conducted with $Re = 4.12 \times 10^{-2}$ and $S = 3.97 \times 10^{-1}$. In each image fluid flows from top to bottom and simulation times are indicated at the bottom of each frame. In both cases the disperse phase is Newtonian. In the case where the continuous phase is shear thinning, the shading represents the local viscosity. (a) Shear thinning continuous phase with $\mu_{c,\infty} = 0$, $\lambda = 1$ and $n = 0.2$ and (b) Newtonian continuous phase with $\mu_c = 0.1$.

The shading of Fig. 6a shows that at the entrance to the contraction, the viscosity within the continuous phase is around $\mu_c = \mu_c^*/\mu_d^* = 0.1$ or less. This is considerably lower than in the previous shear thinning disperse phase simulations where the continuous phase was Newtonian with a viscosity of $\mu_c = 1$. Also, the viscosity of the Newtonian disperse phase in Fig. 6a is now $\mu_d = 1$, considerably higher than in the previous shear thinning disperse phase simulations where generally $\mu_d \lessapprox 0.1$ in this region. The net effect of these differences is that even though the strain rates in the continuous phase in Fig. 6a are higher than in previous simulations, the stress that acts over the interface between the phases generates less strain in the disperse phase than previously. Consequently, the droplet deforms less prior to entering the contraction, and enters the contraction at a later time than in the comparable shear thinning disperse phase simulation of Fig. 5a.

The droplet of Fig. 6a also appears to 'contact' the contraction 'lip' as it enters the contraction. Two factors encourage this apparent 'contact': Firstly, the viscosity of the continuous phase near the contraction lip is very low, around $\mu_c = 0.01$ or less. This means that the film of continuous phase liquid that exists between the contraction wall and droplet can drain away more quickly than in previous cases where the continuous phase was Newtonian. Secondly, the lip at the entrance to the contraction is sharply angled. At a sharply angled corner only a small amount of continuous phase fluid need drain away from the solid for contact between the disperse and solid phases to occur. Indeed, the geometry of the contraction used in these simulations is ideal for promoting surface interactions between the droplet and the solid walls (Rosengarten et al., 2006).

Examining Fig. 6a closely we also see that at times beyond $t = 0.36$ there is an almost continuous film of disperse phase liquid moving slowly downwards along the contraction wall. This is despite the wall being modelled as completely non-wetting with respect to the droplet liquid. As noted above, droplet liquid comes into close contact with the solid at the entrance to the contraction. Below the contraction lip the axial velocity of this liquid is low, as the viscosity of the droplet is relatively high, and the axial velocity along these contraction walls is zero as a result of the no-slip boundary condition. Consequently, droplet liquid that is within the contraction and near its walls takes longer to move through the contraction than liquid closer to its centreline, with the result that a thin film of disperse phase fluid remains 'attached' to the contraction walls long after the majority of the droplet liquid has exited the contraction. As this liquid slowly drains into the outlet region, it forms a disjointed 'bubble' above the main body of disperse phase fluid that is just discernible in the figures at $t = 0.72$ and 0.8.

Analogous to the way in which we used a single characteristic Newtonian viscosity to classify shear thinning disperse phase behaviour, shear thinning continuous phase behaviour can also be described using a single characteristic viscosity. For a shear thinning continuous phase simulation the characteristic viscosity is defined as the viscosity of a Newtonian fluid which when substituted for the shear thinning phase produces similar droplet deformation behaviour. For the simulation of Fig. 6a for example the characteristic viscosity was found by numerical experimentation to be $\mu_c \approx 0.1$. This viscosity is higher than the average shear thinning continuous phase viscosity found within the contraction, so in contrast with the shear thinning disperse phase simulations, the characteristic viscosity cannot be estimated from shear thinning simulation results alone.

Fig. 6b shows results from a simulation performed using a Newtonian continuous phase with this characteristic viscosity. Although the behaviours of both droplets are reasonably similar, there are some differences between the simulations that result from differences in the continuous phase viscosity fields experienced by each. For example, the droplet of Fig. 6b deforms more as it enters the contraction than the droplet of Fig. 6a: At $t = 0.20$ the droplet in the Newtonian case is more 'arrow' shaped and extends further into the contraction than the droplet in the shear thinning case does. This is because the viscosity of the continuous phase is higher around the high shear 'lip' region in the Newtonian simulation than in the shear thinning simulation, which results in greater stress being applied to the droplet in the Newtonian case as it enters the contraction. Conversely, in the outlet region the droplet surrounded by the Newtonian phase is generally more elongated than that surrounded by the shear thinning phase (see $t \geqslant 0.72$). This is because the continuous phase viscosity within the outlet region of the Newtonian simulation is generally lower than that within the outlet region of the shear thinning simulation, resulting in less stress being applied to shorten the axial length of the drop as it exits the contraction in the Newtonian case than in the shear thinning case.

Selected results from other simulations conducted with the same shear thinning continuous phase and Newtonian disperse phase fluids, but employing a variety of *Re* and *S* values, are shown in Fig. 7. Also shown is a *Ca* versus *We* phase chart. Case (b) of this figure is the simulation of Fig. 6a. Case (c), which is very similar to

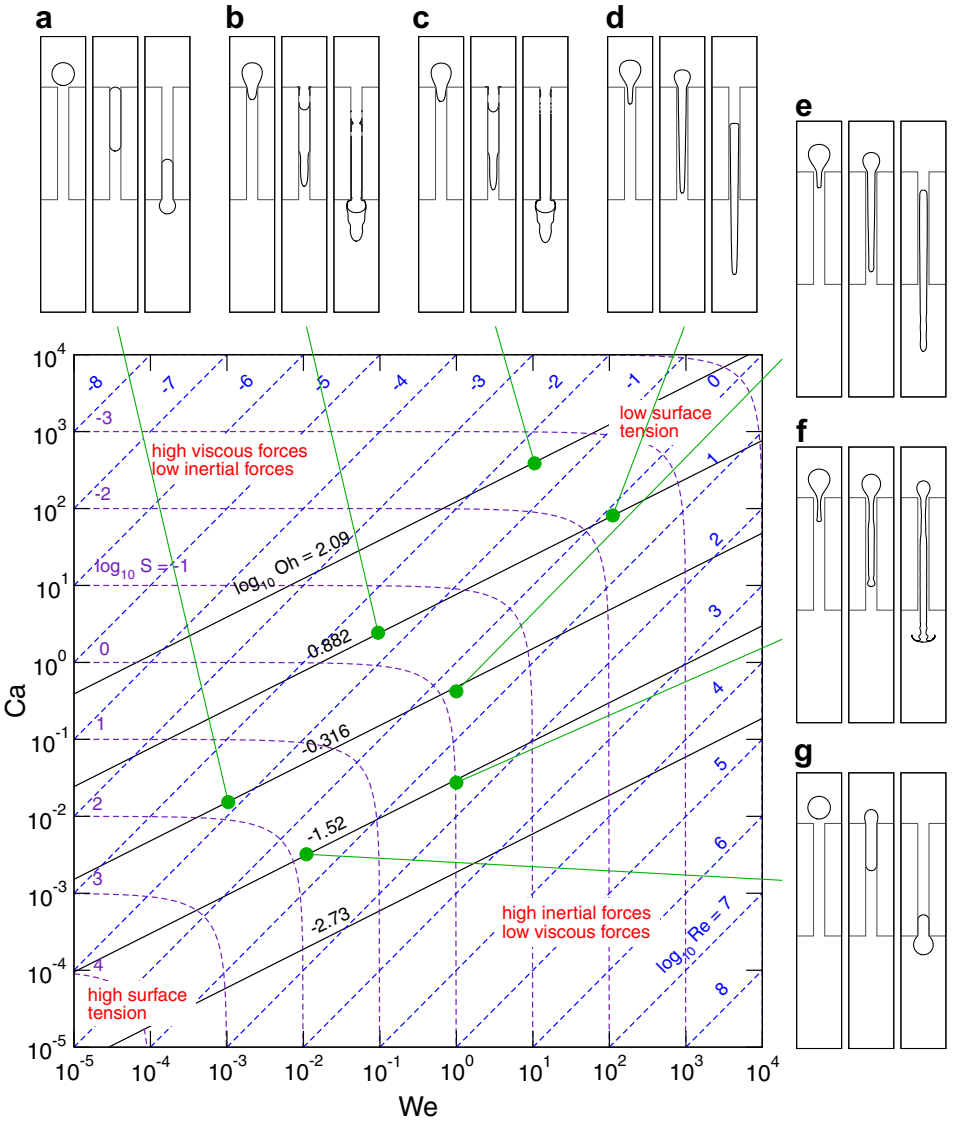

Fig. 7. A phase chart of droplet deformation behaviour. Here the disperse phase is Newtonian and the continuous phase is shear thinning with $\mu_{c,\infty} = 0$, $\lambda = 1.0$ and $n = 0.2$. The dimensionless groups and displayed times for each case are: (a) $Re = 6.59 \times 10^{-2}$, $S = 6.18 \times 10^{1}$, $t = 0.20, 0.40, 0.60$; (b) $Re = 4.12 \times 10^{-2}$, $S = 3.95 \times 10^{-1}$, $t = 0.20, 0.40, 0.70$; (c) $Re = 2.57 \times 10^{-2}$, $S = 2.51 \times 10^{-3}$, $t = 0.20, 0.40, 0.70$; (d) $Re = 1.30 \times 10^{0}$, $S = 5.66 \times 10^{-3}$, $t = 0.20, 0.40, 0.60$; (e) $Re = 2.08 \times 10^{0}$, $S = 6.76 \times 10^{-1}$, $t = 0.20, 0.40, 0.60$; (f) $Re = 3.33 \times 10^{1}$, $S = 9.71 \times 10^{-1}$, $t = 0.20, 0.40, 0.60$; (g) $Re = 3.33 \times 10^{0}$, $S = 7.69 \times 10^{1}$, $t = 0.20, 0.40, 0.70$. In each image fluid flows from top to bottom.

case (b) despite having a significantly smaller surface tension number, demonstrates that surface tension forces are not significant in either cases (b) or (c). When S is higher, for example in cases (a) and (g), the droplet changes shape only when constrained by the contraction walls, similar to other high S cases discussed elsewhere (Harvie et al., 2005, 2006).

When inertia forces are more prevalent, for example in cases (d)–(f) of Fig. 7, the apparent 'contact' between the disperse and solid phases that was observed in the low Re cases does not occur. Instead, these droplets extend into fine filaments while entering the contraction, and accelerate along the centreline as they move through the contraction. Although they take some time to decelerate after exiting the contraction, when they do so the rate of deceleration is rapid. This is because once the shear rate of a shear thinning fluid decreases, its viscosity increases, thus further decreasing its shear rate and increasing its viscosity in a nonlinear fashion. The

leading tip of the droplet in case (f) displays the results of this rapid outlet region deceleration: The tip of this droplet effectively hits a 'wall' of high viscosity continuous phase fluid at approximately three contraction diameters from the contraction exit. This causes the disperse phase fluid to spread radially at this point, forming the 'compacted arrow' shape shown in the final timeframe of the figure.

6. Conclusions

Simulations of a droplet passing through an axisymmetric contraction were performed using a Volume of Fluid algorithm. As a continuation to the companion studies of Harvie et al. (2005, 2006), only liquid–liquid systems were considered and either the disperse or continuous phase was modelled as a shear thinning fluid.

In cases where the disperse phase was shear thinning, the local viscosity of the droplet decreased as it entered the contraction, remained low while within the contraction, and increased as it exited. As a result, the behaviour of these droplets is similar to that of Newtonian droplets having a low 'characteristic' viscosity and passing through the same contraction. Numerical experimentation showed that an appropriate value for this characteristic viscosity is the average viscosity of the shear thinning fluid while within the contraction. While this viscosity cannot be accurately calculated prior to performing a shear thinning simulation, a range in which it lies can be calculated using the results of a Newtonian fluid simulation.

In cases where the continuous phase was shear thinning and the droplet Newtonian, the droplets tended to deform less than their shear thinning cousins when entering the contraction. Also, in simulations where viscous forces dominated inertial forces, apparent 'contact' between the droplet and contraction lip often occurred at the contraction entrance, despite the wall being modelled as non-wetting with respect to the disperse phase. A characteristic viscosity can also be used to describe the shear thinning behaviour of the continuous phase in these simulations; however, this viscosity is not equivalent to the average viscosity of the shear thinning fluid while within the contraction. No estimate or range for this viscosity can be calculated without performing a complete shear thinning simulation.

Acknowledgement

This research was supported by the Australian Research Council Grants Scheme.

References

Aboubacar, M., Matallah, H., Tamaddon-Jahromi, H.R., Webster, M.F., 2002. Numerical prediction of extensional flows in contraction geometries: hybrid finite volume/element method. J. Non-Newtonian Fluid Mech. 104, 125–164.

Anna, S.L., Bontoux, N., Stone, H.A., 2002. Formation of dispersions using 'flow focusing' in microchannels. Appl. Phys. Lett. 82, 364–366.

Barnes, H.A., Hutton, J.F., Walters, K., 1989. An Introduction to Rheology. Elsevier Science.

Bird, R.B., Armstrong, R.C., Hassager, O., 1987. Dynamics of polymeric liquids. In: Fluid Mechanics, vol. 1. John Wiley and sons.

Davidson, M.R., Cooper-White, J.J., 2006. Pendant drop formation of shear-thinning and yield stress fluids. Appl. Math. Modell. 30, 1392–1405.

Eggers, J., 1997. Nonlinear dynamics and breakup of free-surface flows. Rev. Mod. Phys. 69, 865–929.

Gijsen, F.J.H., van de Vosse, F.N., Janssen, J.D., 1998. Wall shear stress in backward-facing step flow of a red blood cell suspension. Biorheology 35, 263–279.

Harvie, D.J.E., Davidson, M.R., Cooper-White, J.J., Rudman, M.J., 2005. A numerical parametric study of droplet deformation through a microfluidic contraction. ANZIAM J. 46 E, C150–C166.

Harvie, D.J.E., Davidson, M.R., Cooper-White, J.J., Rudman, M.J., 2006. A parametric study of droplet deformation through a microfluidic contraction: low viscosity Newtonian droplets. Chem. Eng. Sci. 61, 5149–5158.

Jeong, W., Kim, J., Kim, S., Lee, S., Mensing, G., Beebe, D.J., 2004. Hydro-dynamic microfabrication via 'on the fly' photopolymerization of microscale fibers and tubes. Lab Chip 4, 576–580.

Khayat, R.E., Luciani, A., Utracki, L.A., 1997. Boundary-element analysis of planar drop deformation in confined flow. Part 1. Newtonian fluids. Eng. Anal. Boundary Elem. 19, 279–289.

Khayat, R.E., Luciani, A., Utracki, L.A., Godbille, F., Picot, J., 2000. Influence of shear and elongation on drop deformation in convergent–divergent flows. Int. J. Multiphase Flow 26, 17–44.

Kim-E, M.E., Brown, R.A., Armstrong, R.C., 1983. The roles of inertia and shear-thinning in flow of an inelastic liquid through an axisymmetric sudden contraction. J. Non-Newtonian Fluid Mech. 13, 341–363.

Rosengarten, G., Harvie, D.J.E., Cooper-White, J.J., 2006. Contact angle effects on microdroplet deformation using CFD. Appl. Math. Modell. 30, 1033–1042.

Rudman, M., 1998. A volume-tracking method for incompressible multifluid flows with large density variations. Int. J. Numer. Methods Fluids 28, 357–378.

Song, H., Ismagilov, R.F., 2003. Millisecond kinetics on a microfluidic chip using nanoliters of reagents. J. Am. Chem. Soc. 125, 14613–14619.

Squires, T.M., Quake, S.R., 2005. Microfluidics: fluid physics at the nanoliter scale. Rev. Mod. Phys. 77, 977–1026.

Stone, H.A., 1994. Dynamics of drop deformation and breakup in viscous fluids. Ann. Rev. Fluid Mech. 26, 65–102.

Sugiura, S., Nakajima, M., Seki, M., 2002. Prediction of droplet diameter for microchannel emulsification. Langmuir 18, 3854–3859.

Tanner, R.I., 2000. Engineering Rheology. Oxford University Press.

Tsai, T.M., Miksis, M.J., 1997. The effects of surfactant on the dynamics of bubble snap-off. J. Fluid Mech. 337, 381–410.

Utada, A.S., Lorenceau, E., Link, D.R., Kaplan, P.D., Stone, H.A., Weitz, D.A., 2005. Monodisperse double emulsions generated from a microcapillary device. Science 308, 537–541.